International Journal of Medical, Medicine and Health Sciences
ISSN: 2517-9969
Vol:12, No:6, 2018

X-Ray Fluorescence Molecular Imaging with Improved Sensitivity for Biomedical Applications

Guohua Cao, Xu Dong

***Abstract*—**X-ray Fluorescence Molecular Imaging (XFMI) holds great promise as a low-cost molecular imaging modality for biomedical applications with high chemical sensitivity. However, for in vivo biomedical applications, a key technical bottleneck is the relatively low chemical sensitivity of XFMI, especially at a reasonably low radiation dose. In laboratory x-ray source based XFMI, one of the main factors that limits the chemical sensitivity of XFMI is the scattered x-rays. We will present our latest findings on improving the chemical sensitivity of XFMI using excitation beam spectrum optimization. XFMI imaging experiments on two mouse-sized phantoms were conducted at three different excitation beam spectra. Our results show that the minimum detectable concentration (MDC) of iodine can be readily increased by five times via excitation spectrum optimization. Findings from this investigation could find use for in vivo pre-clinical small-animal XFMI in the future.

***Keywords*—**Molecular imaging, X-ray fluorescence, chemical sensitivity, X-ray scattering.

I. Introduction

XFMI is an imaging technique for elemental mapping. It has potential use for bio-distribution studies of a target molecule in a biological body, which has a great relevance for applications in personal or precision medicine for many diseases such as cancers. Despite some recent progresses, the XFMI technique still needs research to improve its sensitivity at a reasonably low radiation dose. For instance, Jones et al. successfully built a benchtop cone beam x-ray fluorescence CT system in 2012 [1], Kuang et al. utilized the XFMI technique to trace the distributions of three different elements simultaneously in 2013 [2], Ren et al. implemented a pixel-mapping based XFMI for element analysis in 2014 [3], and Yoon et al. developed a three dimensional (3D) Fluorescence Computed Tomography system with CdTe detector array in 2016 [4]. Most of the XFMI techniques utilized the K-shell fluorescence signals to obtain the element distribution, but XFMI using the L-shell fluorescence signals has also been investigated [5]-[7].

The sensitivity of the XFMI technique depends on a number of factors, including the targeted contrast agent, excitation x-ray spectrum, and acquisition geometry. XFMI imaging at different acquisition configurations has been investigated in several recent studies [1]-[4], [8]-[12]. For imaging contrast agent, iodine [13], [14] and gold nanoparticles [15], [16] have been more extensively investigated because of their suitable x-ray fluorescence energies, high x-ray fluorescence yield, and good biochemical properties. A comprehensive comparison of different materials as XFMI contrast agents for biological applications can be found in [17].

One of the main factors that determine the chemical sensitivity in laboratory x-ray source based XFMI is the scattered x-ray background from the interactions between a polychromatic excitation x-ray beam and the imaged object. Many methods have been proposed to overcome the interfering scattered background x-ray photons. For example, the detector is typically placed perpendicular to the direction of the excitation x-ray beam to minimize the amount of scattered x-ray photons reaching the detector [18], and detector collimators are usually used to further reject the number of scattered photons reaching the detector [19]. Various data processing techniques based on curve fitting and statistical modeling have also been applied to subtract the scattered background x-ray photons [7]-[9].

Previously, we have demonstrated that the chemical sensitivity in the XFMI of iodine-based contrast agent using a bremsstrahlung x-ray source can be improved via excitation spectrum optimization with simple x-ray filtrations [13]. Here, we report our systematic and quantitative experimental investigations on improving the chemical sensitivity in XFMI of iodine distribution in mouse-sized phantoms via excitation spectrum optimization, with the goal of applying this technique for *in vivo* small-animal XFMI.

II. Experiments

To investigate the effects of the excitation beam spectra on the chemical sensitivity of XFMI systems, we developed a bench-top XFMI setup using a laboratory bremsstrahlung x-ray source. A picture of the XFMI setup is shown in Fig. 1. The experimental parameters are listed in Table I. The experiments were carried out using three different excitation spectra and two mouse-sized phantoms (a calibration phantom and a contrast phantom). We also developed a theoretical model for our XFMI system, with the total number of measured x-ray photons at the fluorescence energy range as

$$N_{cs}^{measure} = \frac{1}{4\pi} * \int N_{cs} d\Omega = \frac{1}{2} \int_{\theta_d - \frac{\Delta\theta}{2}}^{\theta_d + \frac{\Delta\theta}{2}} N_{cs} \, sin(\theta) \, d\theta \quad (1)$$

with $N_{fl}^{measure}$, $N_{cs}^{measure}$, and $N_{rs}^{measure}$ as the corresponding measured fluorescence photons, Compton scattered photons,

This work was supported in part by Dr. Guohua Cao's CAREER award from the U.S. National Science Foundation (CBET 1351936).

Xu Dong is with Department of Biomedical Engineering and Mechanics, Virginia Polytechnic Institute and State University, Blacksburg, VA 24061 USA.

Guohua Cao is with Department of Biomedical Engineering and Mechanics, Virginia Polytechnic Institute and State University, Blacksburg, VA 24061 USA (corresponding author, e-mail: ghcao@vt.edu).

and Rayleigh scattered photons, all at the x-ray fluorescence energy range. The detailed equations for each term are

$$N_{fl}^{measure} = \frac{1}{4\pi}\int N_{fl}\,d\Omega = \frac{1}{2}\int_{\theta_d-\frac{\Delta\theta}{2}}^{\theta_d+\frac{\Delta\theta}{2}} N_{fl}\sin(\theta)\,d\theta, \quad (2)$$

$$N_{cs}^{measure} = \frac{1}{4\pi}\int N_{cs}\,d\Omega = \frac{1}{2}\int_{\theta_d-\frac{\Delta\theta}{2}}^{\theta_d+\frac{\Delta\theta}{2}} N_{cs}\sin(\theta)\,d\theta, \quad (3)$$

$$N_{rs} = \int_{E_p-\frac{\Delta E}{2}}^{E_p+\frac{\Delta E}{2}} N_{(E)}\left(1-\exp\left(-\mu_{rs_{(E)}} * \mathrm{d}\right)\right)dE, \quad (4)$$

$$N_{fl} = \int_{E_k}^{Emax} \eta N_{(E)}\left(1-\exp\left(-\mu_{pe_{(E)}} * c * d\right)\right)dE \quad (5)$$

$$N_{cs} = \int_{E_1}^{E_2} N_{(E)}\left(1-\exp(-\mu_{cs_{(E)}} * \mathrm{d})\right)dE \quad (6)$$

where $N_{(E)}$ is the number of x-ray photons at energy E for a given excitation spectrum, $\mu_{pe_{(E)}}, \mu_{cs_{(E)}}$, and $\mu_{rs_{(E)}}$ is the photoelectric attenuation coefficient, Compton scattering coefficient, and Rayleigh scattering coefficient of the interacting material at energy E, respectively, and c is the element chemical concentration, d is the attenuating length of the pixel, and η is the fluorescence yield of the target element.

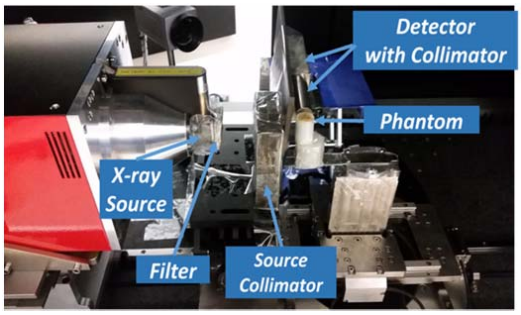

Fig. 1 A picture of the experimental setup

The data acquisition procedures for the physical phantoms experiments are described as follows. For the calibration phantom, only the center voxel of 3 mm × 3 mm × 3 mm, which corresponds to the center vial containing the iodine solution, was imaged in the experiment. All the three filter options were used. The calibration phantom was aligned with the excitation beam path and the detector line of sight in such a way that only the signal generated from the vail containing iodine solutions was able to reach the detector. At each experiment, the center vial was filled with iodine solutions of various concentrations (1%, 0.5%, 0.25%, 0.167%, 0.125%, 0.1% and 0% (pure water) by weight (wt.)). The exposure time for each experiment using different excitation spectrum was pre-determined by the desired surface entrance dose level (D), which typically ranged from 15 seconds to 60 seconds.

TABLE I
PARAMETERS OF THE XFMI EXPERIMENTS

Source to object distance	45 mm
Object to detector distance	30 mm
Collimators aperture size	3 mm
Phantom diameter	20 mm
Phantom vial size	3 mm
Translational step size	3 mm
Source voltage	40 kV
Radiation Dose level	2 mGy for calibration phantom 5 mGy for contrast phantom

III. Data Processing

The iodine x-ray fluorescence signal contains two iodine fluorescence peaks, namely the k_α peak and the k_β peak. The centers of the two peaks are located at 28.6 keV and 32.3 keV, respectively. We set the window width for both fluorescence peaks at 2 keV in our data processing procedure. Therefore, the energy range from 27.6 keV to 29.6 keV was considered as the k_α *fluorescence peak energy range*, and the energy range from 31.3 keV to 33.3 keV was considered as the k_β fluorescence peak energy range. All the other data outside the two fluorescence peak energy ranges were considered the *off-peak energy range* data.

The first step in extracting the *net fluorescence signal* from a measured x-ray fluorescence signal is to find out the *scatter background signals* in the fluorescence peak energy ranges. For the off-peak energy range data, a ten-order polynomial least-squares fit was applied to obtain the *off-peak background fit*. Then, the scatter background signals within the fluorescence peak energy ranges were obtained by the ten-order polynomial interpolations of the off-peak background fit. The interpolated scatter background signals (denoted as bg) were subtracted from the measured x-ray fluorescence signals at the fluorescence peak energy range to obtain the net fluorescence signal. In this study, we only used iodine fluorescence signal at the k_α peak, because the intensity of the k_β peak is barely visible in our low dose experiments.

After obtaining the net iodine fluorescence signal, it was fit with a Gaussian curve. The height (denoted as h) of the fitted Gaussian curve was taken as the *strength* of the net fluorescence signal, and hereafter it is referred as the *fluorescence peak height*. The fluorescence peak height was corrected by an attenuation correction factor, which takes account of the attenuation from the fluorescence origination site to the detector, to obtain the XFMI signal in the final XFMI images.

The Minimum Detectable Concentration (MDC) is used in the study to characterize the chemical sensitivity of a XFMI system, which is a measure of the capability of the system to distinguish a net fluorescence signal (the fluorescence peak height (h)) from the random fluctuations of the background signal (bg). The random fluctuations of the background signal can be characterized by the background noise (σ_{bg}), which was treated as the mean of all the deviations between the experimentally measured data points and the fitted background values at the off-peak energy range. To be treated as distinguishable from the background fluctuations with 95%

confidence level, the fluorescence peak height (h) must be larger than $1.96\sigma_{bg}$. Based on the data from the calibration phantom, a least squares linear fit was applied to the fluorescence peak heights obtained at various iodine concentrations. The MDC is determined by the intersecting point between the linear fit line and the $1.96\sigma_{bg}$ reference line.

IV. Results

The two XFMI images for the contrast phantom are shown in Fig. 2. The linearity between the XFMI signal intensity and iodine is confirmed from the result in Fig. 3. The best sensitivity that we have obtained is 0.074% (by weight) of iodine via 1.02-mm Cu filtration, which is 5 times more sensitive than that from the 2.08-mm Al filtration, as shown in Table II. As shown in Fig. 3, excellent linearity is observed ($\boldsymbol{R^2 > 0.97}$ for both fits), which indicates the high confidence of our XFMI technique in accurately mapping out the different iodine concentrations in single XFMI experiment.

Using the data from the calibration phantom, the MDCs were obtained for the three filter options. The best sensitivity (i.e. MDC with smallest value) came from the excitation spectrum by the 1.02-mm Cu filter, with the MDC as low as 0.074%, as listed in Table II. Compared to the MDC from the excitation spectrum by the 2.08 mm Al filter, the MDC from the excitation spectrum by the 5.20 mm Al filter was improved 2.22 times, and the MDC from the spectrum by the 1.02 mm Cu filer was improved 5.26 times. This demonstrates that the sensitivity of a XFMI system can be significantly increased by optimizing its excitation spectrum. The intersection points of these 95% confidence level lines with the $\boldsymbol{1.96\sigma_{bg}}$ reference line can be used to find out the uncertainties of the derived MDCs, which are shown in Table II.

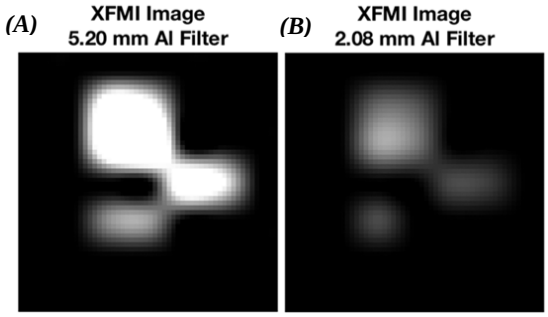

Fig. 2 The XFMI images generated from the pixel-mapping method for the contrast phantom at two excitation spectra. The display window for the both images is [0, 40]

V. Discussion and Conclusion

In this study, we experimentally investigated the impact of the excitation x-ray spectrum on the chemical sensitivity of XFMI in a pixel-mapping configuration. We investigated the effects of three distinctive excitation spectra, which were generated by changing the material and thickness of the x-ray source filter, on the XFMI imaging of a calibration phantom and a contrast phantom containing iodine solutions at low concentrations. We quantitatively determined the chemical sensitivity of the XFMI system using the MDC of iodine. Our experimental results exhibit strong linearity between the fluorescence peak height and iodine concentration for the calibration phantom, as well as between the XFMI signal and iodine concentration for the contrast phantom. The strong linearity gives us high confidence in the accuracy of mapped iodine concentrations from our XFMI experiments.

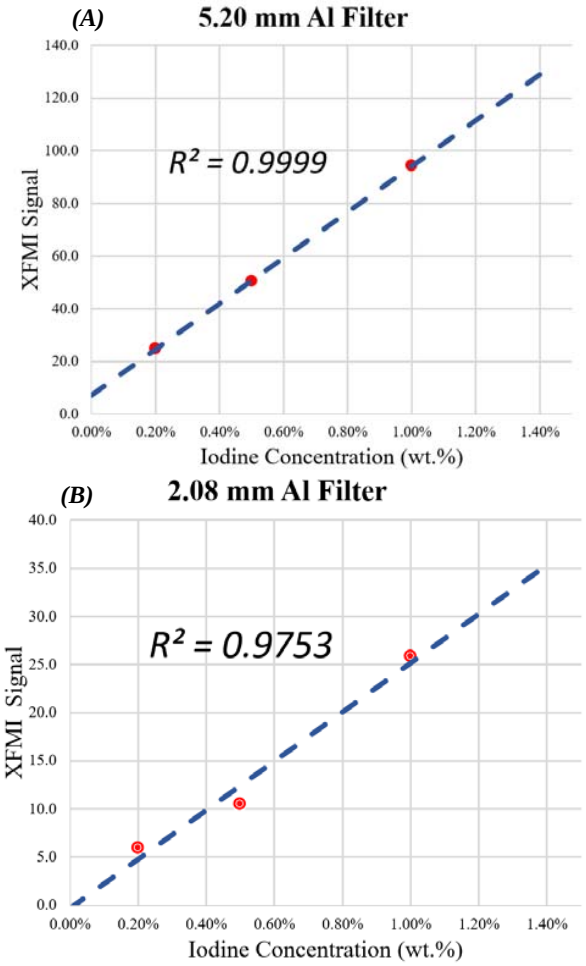

Fig. 3 Linearity between the XFMI image signals and the iodine concentrations for the two XFMI experiments with (A) 5.20-mm Al filter, and (B) 2.08-mm Al filter

TABLE II
The MDCs at Three Excitation Spectra

Excitation spectra	MDC ($wt.$)
1.02-mm Cu filter:	$0.074\%\ ^{-0.043\%}_{+0.051\%}$
5.20-mm Al filter:	$0.175\%\ ^{-0.059\%}_{+0.072\%}$
2.08-mm Al filter:	$0.389\%\ ^{-0.146\%}_{+0.225\%}$

We investigated the MDCs under different excitation spectra for a fixed surface entrance radiation dose level of 2 mGy. The result showed that increasing the thickness of the x-ray source filter (from 2.08 mm All to 5.20 mm Al) led to 2.22 times improvement in the chemical sensitivity, and when switching

the filter to material with a higher atomic number (from 2.08 mm Al to 1.02 mm Cu), the chemical sensitivity was increased 5.26 times. The results are in line with what one would expect. To the best of our knowledge, our sensitivity is the among the highest among those reported laboratory x-ray source based XFMI techniques [1]-[4], [8]-[12], especially when compared at the mGy level of radiation dose as reported here.

The sensitivity in our XFMI setup can be further improved with a better optimized excitation spectrum. There are at least two possible approaches. One is to increase the x-ray tube voltage to get more effective x-rays that are capable of generating fluorescence signals. Another is to further optimize the excitation spectrum by more filtering, for instance using a thicker copper filter to obtain a larger percentage of effective x-rays. However, for the first approach, the efficiency of exciting x-ray fluorescence in the target element by an excitation photon will decrease as the energy of the excitation photon increases, which will lead to lower dose efficiency (defined as sensitivity normalize by the radiation dose); for the second approach, heavier filtration to the excitation beam can lead to higher sensitivity but at a cost of reduced excitation x-ray beam intensity, which would lead to longer exposure time to obtain the same amount of fluorescence signals. Therefore, for a given imaging task, a tradeoff between the excitation beam filtration, exposure time, and radiation dose has to be made.

The goal of this work is to lay a foundation for building a XFMI device that can perform molecular imaging in live animals in longitudinal studies. To accomplish this goal, the XFMI imaging technique should obtain a sufficient level of molecular sensitivity, spatial resolution, acquisition time, and radiation dose. We understand that obtaining a high molecular sensitivity only fulfills part of these requirements. Furthermore, there are many tradeoffs between these different requirements (e.g. sensitivity and resolution, etc.). Here, we put the radiation dose and sensitivity at the foremost requirements that need to be accomplished for a future *in vivo* XFMI experiment. The spatial resolution could be relaxed a bit, because there are many other complementary and high-resolution imaging techniques available such as micro-CT, and the acquisition time can be shortened with an industrial-grade x-ray source with high power. Even for just the requirements in sensitivity and radiation dose, we believe that there could be further room to improve. Our future research plan is to build a software model based on the theoretical model described in Section II and validated by the experimental measurements reported in this study, so that an *optimum* excitation spectrum from a bremsstrahlung x-ray source can be calculated from the software model for a given XFMI experiment with a targeted trace element in a given geometrical configuration.

In conclusion, a systematic experimental investigation of the effect of the x-ray excitation spectrum on the chemical sensitivity of the XFMI system has been reported in this work. The results show that, under optimized excitation beam, the chemical sensitivity of the XFMI system was greatly improved. Findings from this investigation could potentially find use for *in vivo* pre-clinical small-animal XFMI in the future.

REFERENCES

[1] Jones, B. L., et al., Experimental demonstration of benchtop x-ray fluorescence computed tomography (xfct) of gold nanoparticle-loaded objects using lead- and tin-filtered polychromatic cone-beams. Phys Med Biol, 2012. 57(23): p. N457-67.
[2] Kuang, Y., et al., First demonstration of multiplexed x-ray fluorescence computed tomography (xfct) imaging. IEEE transactions on medical imaging, 2013. 32(2): p. 262-267.
[3] Ren, L., et al., Three-dimensional x-ray fluorescence mapping of a gold nanoparticle-loaded phantom. Med Phys, 2014. 41(3): p. 031902.
[4] Yoon, C., Y. Kim, and W. Lee, *3d non-destructive fluorescent x-ray computed tomography with a cdte array.* IEEE Transactions on Nuclear Science, 2016. 63(3): p. 1844-1853.
[5] Bazalova, M., et al., L-shell x-ray fluorescence computed tomography (xfct) imaging of cisplatin. Phys. Med. Biol, 2014. 59(1): p. 219-232.
[6] Bazalova-Carter, M., et al., Experimental validation of l-shell x-ray fluorescence computed tomography imaging: Phantom study. Journal of Medical Imaging, 2015. 2(4): p. 043501-043501.
[7] Manohar, N., F.J. Reynoso, and S.H. Cho, Experimental demonstration of direct l-shell x-ray fluorescence imaging of gold nanoparticles using a benchtop x-ray source. Medical physics, 2013. 40(8).
[8] Cong, W., H. Shen, and G. Wang, Spectrally resolving and scattering-compensated x-ray luminescence/fluorescence computed tomography. Journal of biomedical optics, 2011. 16(6): p. 066014-066014-7.
[9] Ricketts, K., et al., A quantitative x-ray detection system for gold nanoparticle tumour biomarkers. Phys Med Biol, 2012. 57(17): p. 5543-55.
[10] Ahmad, M., et al., Order of magnitude sensitivity increase in x-ray fluorescence computed tomography (xfct) imaging with an optimized spectro-spatial detector configuration: Theory and simulation. IEEE Trans Med Imaging, 2014. 33(5): p. 1119-28.
[11] Ahmad, M., et al., Optimized detector angular configuration increases the sensitivity of x-ray fluorescence computed tomography (xfct). IEEE Trans Med Imaging, 2015. 34(5): p. 1140-7.
[12] Wu, D., et al. Measurements of gold nanoparticle concentration with k-shell x-ray fluorescence spectrum. in Proc. of SPIE Vol. 2017.
[13] Cao, G., J. Lu, and O. Zhou. X-ray fluorescence molecular imaging with high sensitivity: Feasibility study in phantoms. in SPIE Medical Imaging. 2012. International Society for Optics and Photonics.
[14] Takeda, T., et al., *Iodine imaging in thyroid by fluorescent x-ray ct with 0.05 mm spatial resolution.* Nuclear Instruments and Methods in Physics Research Section A: Accelerators, Spectrometers, Detectors and Associated Equipment, 2001. 467: p. 1318-1321.
[15] Wu, D., et al., A method of measuring gold nanoparticle concentrations by x-ray fluorescence for biomedical applications. Medical physics, 2013. 40(5).
[16] Larsson, J. C., et al. High-spatial-resolution nanoparticle x-ray fluorescence tomography. in Medical Imaging 2016: Physics of Medical Imaging. 2016. International Society for Optics and Photonics.
[17] Shilo, M., et al., Nanoparticles as computed tomography contrast agents: Current status and future perspectives. Nanomedicine, 2012. 7(2): p. 257-269.
[18] Ricketts, K., et al., *A bench-top k x-ray fluorescence system for quantitative measurement of gold nanoparticles for biological sample diagnostics.* Nuclear Instruments and Methods in Physics Research Section A: Accelerators, Spectrometers, Detectors and Associated Equipment, 2016. 816: p. 25-32.
[19] Takeda, T., et al. Fluorescent x-ray computed tomography with synchrotron radiation using fan collimator. in Proc. SPIE. 1996.